Available online at www.sciencedirect.com
ScienceDirect
Trans. Nonferrous Met. Soc. China 26(2016) 1201−1210
Transactions of Nonferrous Metals Society of China
www.tnmsc.cn

Enhancing corrosion resistance of 7150 Al alloy using novel three-step aging process

Rui-ji SUN[1], Qing-qing SUN[1,2,3], Yue-huang XIE[1], Peng-xuan DONG[1], Qi-yuan CHEN[2], Kang-hua CHEN[1]

1. State Key Laboratory of Powder Metallurgy, Central South University, Changsha 410083, China;
2. School of Chemistry and Chemical Engineering, Central South University, Changsha 410083, China;
3. School of Chemical Engineering, Purdue University, West Lafayette 47907, IN, USA

Received 16 April 2015; accepted 14 December 2015

Abstract: The effects of a novel three-step aging process (T76+T6) on the electrochemical corrosion behavior of 7150 extruded aluminum alloy were evaluated and compared with those of the conventional retrogression and re-aging process (T77). The open circuit potential (OCP), cyclic polarization and electrochemical impedance spectra (EIS) of the Al alloys were measured after treatment in three solutions (3.5% NaCl (mass fraction); 10 mmol/L NaCl + 0.1 mol/L Na_2SO_4; 4 mol/L NaCl + 0.5 mol/L KNO_3 + 0.1 mol/L HNO_3). The parameters including the corrosion potential, pitting potential, pit transition potential and steepness, and potential differences were extensively discussed to evaluate the corrosion behavior of the Al alloys. The electrochemical and scanning electron microscopy (SEM) data show that compared with the 7150-T77 Al alloy, the T76 + T6 aged 7150 Al alloy exhibits better resistance to pitting corrosion, inter-granular corrosion (IGC) and exfoliation corrosion, which is attributed to further coarsening and inter-spacing of the grain boundary particles (GBPs) as revealed by transmission electron microscopy. Furthermore, the hardness tests indicate that an attractive combination of strength and corrosion resistance was obtained for the 7150 Al alloy with T76 + T6 treatment.

Key words: 7150 aluminum alloy; novel three-step aging; cyclic polarization; electrochemical impedance spectroscopy

1 Introduction

7000 series aluminum alloys are extensively used in aeronautical applications due to their ultra-high strength [1]. One limitation of their use in the metallurgical state of the highest strength (commonly called the T6 temper) is the low corrosion resistance of these materials. To date, extensive effort continues to be expended to acquire high corrosion resistance with the least loss of strength. The T7x over-aged temper exhibits enhanced corrosion performance, but at the expense of 10%−15% strength [2]. The retrogression and re-aging (RRA) process proposed by CINA [3] can be applied to increasing the corrosion resistance while maintaining the strength at levels similar to that of the T6 temper. This type of heat treatment comprises an initial aging step that leads to an under-aged or a T6 state. The second step, performed for a short duration at high temperature (called retrogression), dissolves part of the initially formed precipitates. Finally, a third heat treatment step, at lower temperature, leads to the final microstructure. Repetitive-RRA could further improve stress cracking corrosion resistance with the retention of strength compared with the RRA temper [4,5]. However, it is difficult to apply the retrogression of RRA and repetitive-RRA (performed in the range of 180−260 °C for several minutes) to thick plates [6,7]. Recently, a novel three-step aging process has been proposed for application to an Al−Zn−Mg−Cu thick plate [8]. This three-step aging process is similar to RRA, except that the second aging step involves under-treatment for a longer duration at lower temperature. This process reportedly increases the strength combination with fracture toughness, but few studies have focused on the resulting corrosion performance. Investigations of the corrosion behavior of 7000 series aluminum alloys are necessary because these alloys are quite sensitive to

Foundation item: Projects (51134007, 51201186) supported by the National Natural Science Foundation of China; Project (51327902) supported by the Major Research Equipment Development, China; Projects (2012CB619502, 2010CB731701) supported by the National Basic Research Program of China; Project (12JJ6040) supported by the Natural Science Foundation of Hunan Province, China
Corresponding author: Kang-hua CHEN; Tel: +86-731-88830714; E-mail: khchen@csu.edu.cn
DOI: 10.1016/S1003-6326(16)64192-4

localized corrosion and stress cracking corrosion. Enhancing the corrosion resistance of these alloys has been a long-term goal in this field.

The corrosion of Al alloys in neutral 3.5% (mass fraction) NaCl solution has been intensively investigated [9−14]. This medium is similar to a real sea water environment and is particularly suitable for corrosion characterization of shipboard aircraft materials. However, it also shows several limitations such as the absence of a pit transition potential (φ_{ptp}) [15], the lack of variety [16,17], less studied corrosion mechanisms [18,19] and the absence of a pitting potential (φ_{pit}) [15,20]. Understanding the effect of different media on the corrosion behavior of Al alloys is of scientific interest and technological importance. Therefore, the evaluation of corrosion mechanisms using various electrolytes is a worthwhile and necessary undertaking. In this study, three solutions (3.5% NaCl; 10 mmol/L NaCl + 0.1 mol/L Na_2SO_4; 4 mol/L NaCl + 0.5 mol/L KNO_3 + 0.1 mol/L HNO_3 (EXCO)) were selected as electrolytes for electrochemical measurements to investigate the influence of the novel three-step T76 + T6 aging and conventional RRA T77 processes on the corrosion behavior of 7150 extruded Al alloy.

2 Experimental

2.1 Alloys and heat treatments

The investigated material was an extruded 7150 aluminum alloy plate received from Aluminum Corporation of China. The chemical composition (mass fraction) of the plate is listed in Table 1. The samples, cut into 15 mm × 15 mm × 3 mm plates, were solution heat treated for 30 min at 480 °C and then subjected to cold water quenching, followed by the T77 and T76 + T6 aging processes, as shown in Fig. 1.

Table 1 Composition of 7150 Al alloy (mass fraction, %)

Zn	Mg	Cu	Zr	Fe	Si	Al
6.5	2.4	2.2	0.15	0.08	0.061	Bal.

2.2 Hardness and conductivity

The strength of 7150 Al alloy subjected to different aging treatments was evaluated by Vickers hardness tests. The electrical conductivity was determined using an SX1931 digital micrometer. The hardness and conductivity values represent the average of at least five measurements.

2.3 Electrochemical measurements

For electrochemical characterization, the samples were wet ground with successive grades of silicon carbide abrasive paper (from P240 to P1500), followed by diamond finishing to 0.1 μm. A CHI 660C

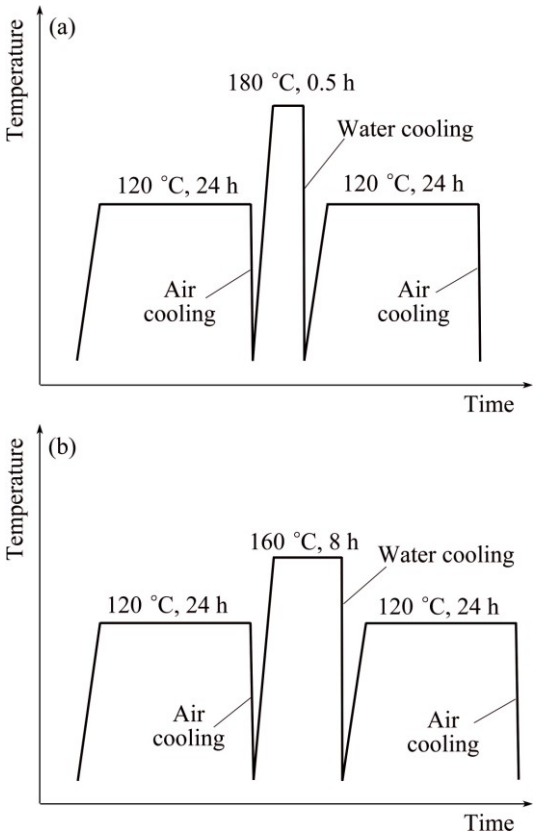

Fig. 1 Schematic diagram of T77 (a) and T76 + T6 (b) aging processes of 7150 Al alloy

electrochemical workstation (Shanghai Chenhua, China) connected to a three-electrode cell was used for the electrochemical measurements. The working electrode comprised the test material with an immersed area of 0.5 cm^2. A platinum plate and a saturated calomel electrode (SCE) were used as the counter and reference electrodes, respectively. The test solutions comprised 3.5% NaCl, 10 mmol/L NaCl + 0.1 mol/L Na_2SO_4 and EXCO (4 mol/L NaCl + 0.5 mol/L KNO_3 + 0.1 mol/L HNO_3), respectively. Open circuit potential (OCP) curves were first acquired. Electrochemical impedance spectroscopy (EIS) measurements were conducted in a Faraday cage after the OCP test. The frequency ranged from 100 kHz to 1 Hz and the amplitude of the sinusoidal potential signal was 10 mV with respect to the OCP. The impedance spectra were analyzed using ZView™ (Scribner Associates Inc.) electrochemical analysis software. Cyclic polarization curves were obtained after the EIS test at a scanning rate of 1 mV/s in the range of −1.0 to −0.2 V. All electrochemical tests were performed in triplicate.

2.4 Microstructure and corrosion morphology

Microstructural analysis was performed via bright field imaging with a TECNAI G^2 20 transmission electron microscope (TEM). The corrosion morphologies

after the cyclic polarization tests were characterized by scanning electron microscopy (SEM).

3 Results

3.1 Open circuit potential

Figures 2(a)−(c) show the OCP curves of 7150 aluminum alloys immersed in 3.5% NaCl, 10 mmol/L NaCl + 0.1 mol/L Na_2SO_4, and EXCO media, respectively. For all electrolytes, the OCP of the T76 + T6 aged 7150 Al alloy is found to be more positive

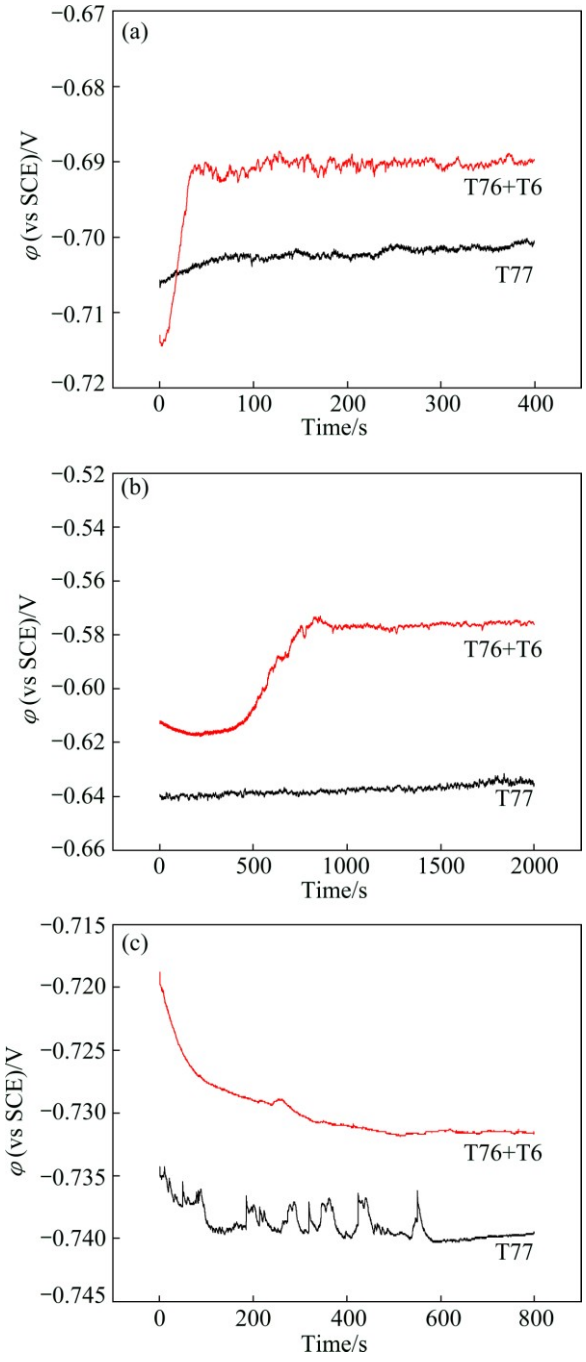

Fig. 2 OCP curves of 7150 Al alloy as function of aging process in 3.5% NaCl (a), 10 mmol/L NaCl + 0.1 mol/L Na_2SO_4 (b) and EXCO (c) media

(anodic) than that of the 7150-T77 Al alloy, indicating a lower tendency towards corrosion for the alloy subjected to T76 + T6 treatment. Moreover, in the EXCO medium (Fig. 2(c)), the significant fluctuation of OCP, corresponding to activation and repassivation of the air-formed oxide film on the alloy surface, was observed for the 7150-T77 sample, also indicating greater susceptibility of this sample to corrosion [21−23].

3.2 Potentiodynamic polarization curves

Figures 3(a)−(c) show the cyclic polarization curves of the 7150 extruded Al alloy immersed in 3.5% NaCl, 10 mmol/L NaCl + 0.1 mol/L Na_2SO_4, and EXCO, respectively, as a function of the respective tempering processes. The parameters derived from the cyclic polarization curves, including the corrosion potential (φ_{corr}), repassivation potential (φ_{rep}), corrosion current density (J_{corr}) corresponding to φ_{corr}, corrosion current density (J_{rep}) corresponding to φ_{rep}, current density (J_{rev}) at the reverse potential, and linear polarization resistances (R_{corr} and R_{rep}) are listed in Tables 2−4.

In all of the evaluated electrolytes, the current densities (J_{corr}, J_{rep} and J_{rev}) of the T76 + T6 aged alloy were lower. These results indicate that the rate of corrosion of the T76 + T6 aged T150 Al alloy is slower than that of the 7150-T77 Al alloy. The current density tends to become constant above the corrosion potential. This corresponds to the limit anodic current density, which is the maximum dissolution rate for the alloy. The T77 aged 7150 Al alloy presents a higher limit anodic current than the T76 + T6 aged 7150 Al alloy in all media. In addition, the current density during the backwards potentiodynamic polarization in the negative direction is lower for the alloy treated with this novel three-step aging technique.

On the basis of mixed-potential theory, the corrosion potential (φ_{corr}) is not a thermodynamic parameter and its value is determined by both the anodic and cathodic branches. For instance, an increase of the cathodic current density should lead to a shift in the corrosion potential of the anodic direction, while an increase of the anodic current density should lead to a shift of the corrosion potential in the cathodic direction. Therefore, φ_{corr} is not a necessary parameter of the rate or tendency of corrosion. However, due to the presence of a passive film on Al, a more negative value of φ_{corr} often corresponds to more "active pits" for the "active pits−passive wall" surface, leading to a greater corrosion tendency. In 3.5% NaCl and EXCO media, the corrosion potential (φ_{corr}) and repassivation potential (φ_{rep}) (where φ_{rep} is also a mixed potential) of the T76 + T6 aged 7150 Al alloy are much more anodic than those of the 7150-T77 Al alloy. Furthermore, it should be noted that the change of φ_{corr} in 10 mmol/L NaCl + 0.1 mol/L

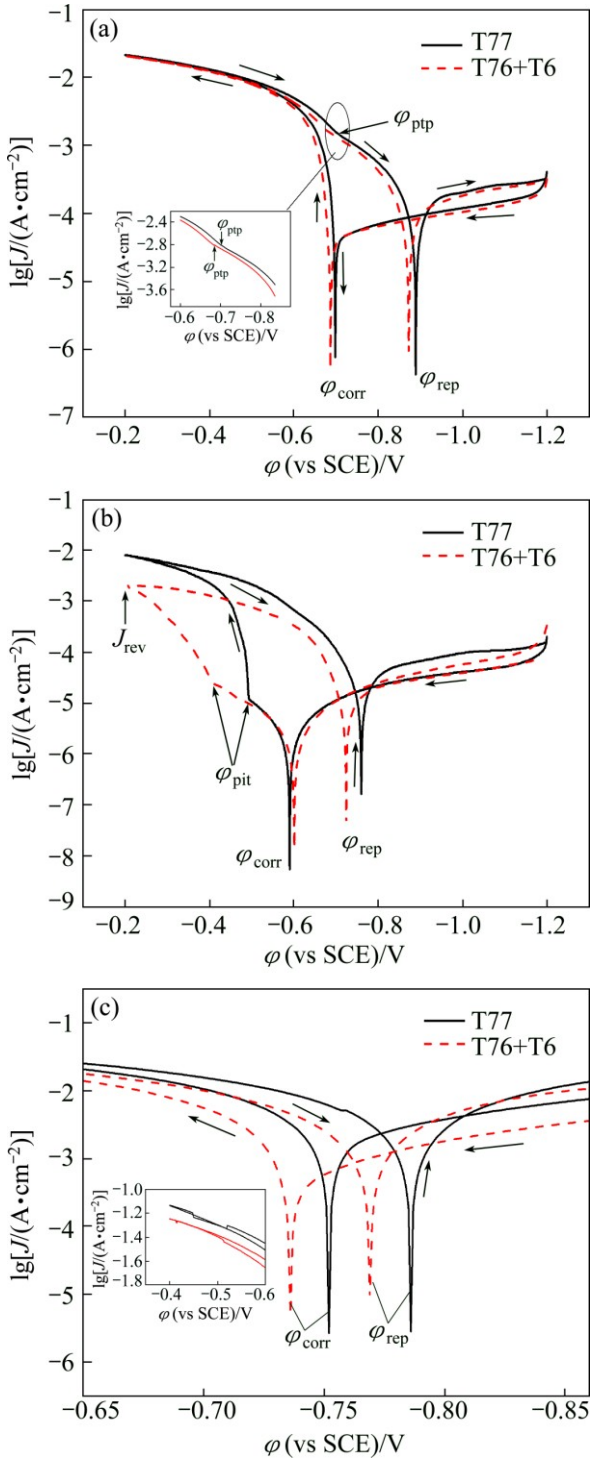

Fig. 3 Cyclic polarization curves of 7150 Al alloy sample subjected to different heat treatments in three corrosive electrolytes: (a) 3.5% NaCl; (b) 10 mmol/L NaCl + 0.1 mol/L Na_2SO_4; (c) EXCO

Na_2SO_4 is not in accordance with that in 3.5% NaCl or EXCO. This is associated with the much less corrosive nature of 10 mmol/L NaCl + 0.1 mol/L Na_2SO_4 compared with other electrolytes. In our previous study, we found that φ_{corr} shifts to the positive direction as the chloride concentration increases within the range of 1−50 mmol/L [24,25]. Overall, all the corrosion values obtained in the three media show that the T76 + T6 treated 7150 Al alloy is less susceptible to corrosion.

The characteristic parameters were determined for the 7150 Al alloy in specific media. For the solution of 10 mmol/L NaCl + 0.1 mol/L Na_2SO_4, one of the remarkable differences compared with other two media is the presence of a pitting potential, the value of which is −0.49 V (vs SCE) for the 7150-T77 Al alloy and −0.407 V (vs SCE) for the T76 + T6 aged 7150 Al alloy. Additionally, a pit transition potential (φ_{ptp}) could be detected in all media, except for EXCO solution. The φ_{ptp} value of the T76 + T6 aged 7150 Al alloy is more anodic than that of the 7150-T77 Al alloy.

3.3 Electrochemical impedance spectroscopy

EIS enables us to determine different parameters of equivalent electrochemical systems (capacitance, resistance, electrolyte interface, etc.). Figures 4(a)−(c) show the electrochemical impedance spectra of the 7150 Al alloy subjected to different tempering processes in 3.5% NaCl, 10 mmol/L NaCl + 0.1 mol/L Na_2SO_4 and EXCO media, respectively.

For accurate analysis of the EIS time-dependent constants of the corrosion process, the equivalent electrical circuits model $R_s(CPE_p(R_{pit}(CPE_{pit}\cdot R_{ct})))$ was used for 7150 Al alloy in 3.5% NaCl and 10 mmol/L NaCl + 0.1 mol/L Na_2SO_4 solutions, while $R_s(CPE_{pit}\cdot R_{ct})$ was used for 7150 Al alloy in EXCO medium, as presented in Fig. 5. The physical meaning of the equivalent circuit elements is described as follows: R_s is the ohmic resistance of the electrolyte, CPE_p is the constant phase element of the passive film, R_{pit} is the film pore resistance, CPE_{pit} is the constant phase element of the double layer, and R_{ct} is the charge transfer resistance.

The element CPE is used to signify the possibility of non-ideal capacitance with varying n (n is an empirical exponent between 0 and 1). Element CPE is commonly used in the case of uneven current distribution at the surface or in the case of increased surface

Table 2 Parameters from cyclic polarization curves of 7150 Al alloy in 3.5% NaCl solution

Temper	φ_{corr} (vs SCE)/V	J_{corr}/(mA·cm^{-2})	R_{corr}/(Ω·cm^{-2})	φ_{rep}(vs SCE)/V	J_{rep}/(mA·cm^{-2})	R_{rep}/(Ω·cm^{-2})	φ_{ptp}(vs SCE)/V	J_{rev}/(mA·cm^{-2})
T77	−0.698	0.514	114	−0.889	0.281	216	−0.705	22.38
T76 + T6	−0.687	0.304	200	−0.872	0.226	236	−0.677	20.51

Table 3 Parameters from cyclic polarization curves of 7150 Al alloy in 10 mmol/L NaCl + 0.1 mol/L Na_2SO_4 solution

Temper	φ_{corr} (vs SCE)/V	J_{corr}/ ($\mu A \cdot cm^{-2}$)	R_{corr}/ ($\Omega \cdot cm^{-2}$)	φ_{rep}(vs SCE)/V	J_{rep}/ ($\mu A \cdot cm^{-2}$)	R_{rep}/ ($\Omega \cdot cm^{-2}$)	φ_{pit}(vs SCE)/V	φ_{ptp}(vs SCE)/V	J_{rep}/ ($mA \cdot cm^{-2}$)
T77	−0.590	3.48	9716	−0.760	0.38	981	−0.490	−0.614	7.94
T76 + T6	−0.601	2.53	5711	−0.724	0.15	948	−0.407	−0.588	1.99

Table 4 Parameters from cyclic polarization curves of 7150 Al alloy in EXCO solution

Temper	φ_{corr} (vs SCE)/V	J_{corr}/ ($mA \cdot cm^{-2}$)	R_{corr}/ ($\Omega \cdot cm^{-2}$)	φ_{rep} (vs SCE)/V	J_{rep}/ ($mA \cdot cm^{-2}$)	R_{rep}/ ($\Omega \cdot cm^{-2}$)	J_{rev}/ ($mA \cdot cm^{-2}$)
T77	−0.752	8.28	6	−0.786	8.62	5	73.45
T76 + T6	−0.736	3.84	11	−0.769	6.63	7	56.75

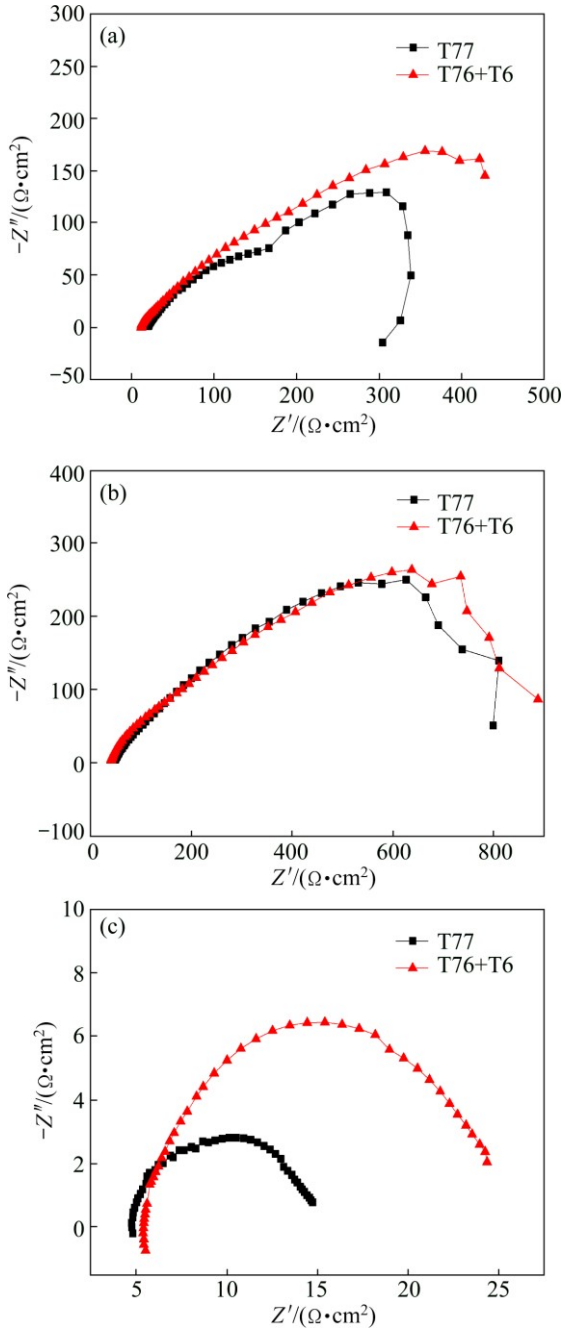

Fig. 4 EIS of 7150 Al alloy in 3.5% NaCl (a), 10 mmol/L NaCl + 0.1 mol/L Na_2SO_4 (b), and EXCO (c) media as function of aging process

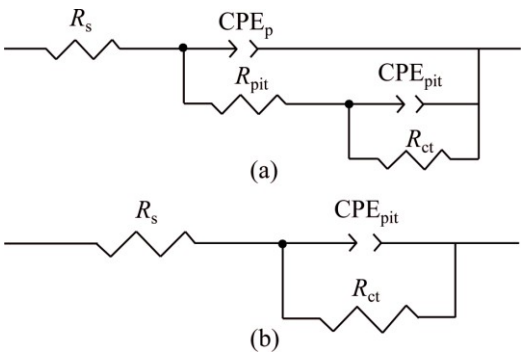

Fig. 5 Equivalent circuits of EIS of 7150 Al alloy in 3.5% NaCl and 10 mmol/L NaCl + 0.1 mol/L Na_2SO_4 (a) and EXCO (b) media

roughness. The impedance of CPE (Z_{CPE}) is a function of the angular frequency (ω) and related to the capacitance (C):

$$Z_{CPE(\omega)}=[Cj\omega^{-n}]^{-1}$$

where $j^2=-1$. When n=1, the CPE represents purely capacitive behavior associated with a perfectly smooth surface. When n=0, the CPE represents a resistor [26].

The polarization resistance (R_p, where $R_p = R_{pit}+R_{ct}$) or charge transfer resistance (R_{ct}) of the Al alloys in the three solutions was plotted as a function of the temper, as shown in Fig. 6. The difference between the polarization resistance of the 7150-T77 and T76 + T6 aged Al alloys is relatively small in trace Cl^--containing solution, as can be seen from Fig. 6(b). The most distinct difference between the R_{ct} of the two tempers was observed in EXCO solution. The EIS data are in good agreement with the OCP curves and cyclic polarization curves.

4 Discussion

Figure 7 shows the corrosion morphologies of the 7150 Al alloy after cyclic polarization tests. Different degrees of corrosion and corrosion mechanisms were observed for the 7150 Al alloy in different corrosive media.

The exposed surfaces in Figs. 7(a_1) and (a_2) reveal

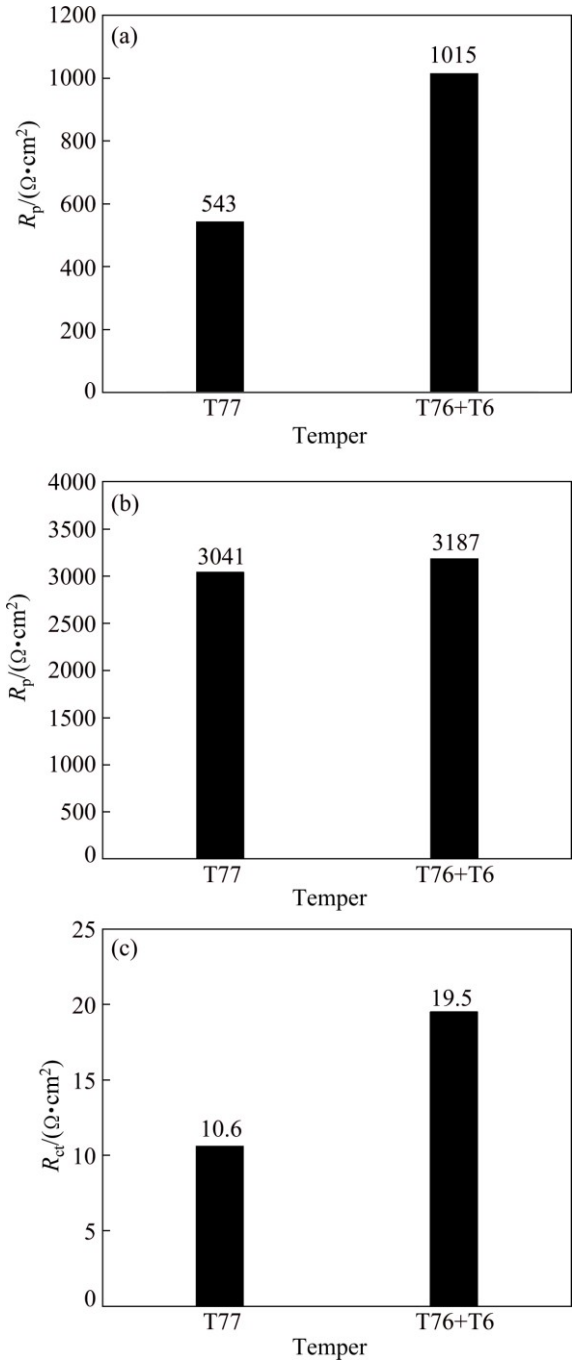

Fig. 6 Polarization resistance or charge transfer resistance of 7150 Al alloy in 3.5% NaCl (a), 10 mmol/L NaCl + 0.1 mol/L Na_2SO_4 (b) and EXCO (c) media as function of temper

inter-granular corrosion along with selective dissolution of the matrix at the intermetallics in 3.5% NaCl. The diameter is 10−20 μm for the larger pits and several micrometers for the smaller pits. It is probable that the pits are formed by fall-out of the intermetallics from the surface due to the dissolution of the surrounding matrix. It is also possible that the pits occur due to selective dissolution of the intermetallics. The Al alloy surfaces are dominated by pitting corrosion in the 10 mmol/L NaCl + 0.1 mol/L Na_2SO_4 medium, as shown in Figs. 7(b_1) and (b_2). The exposed surface shows the evidence of localized attack at the site of intermetallics, caused by the dissolution of the matrix around the intermetallics. Furthermore, a number of pits (~2 μm) containing other white and dark pits are observed in the images. The white pits and the residual corrosion product are caused by the breakdown of the passive film, while the dark pits represent the initial stage preceding film breakdown. In the EXCO medium (Figs. 7(c_1) and (c_2)), exfoliation corrosion does not appear to be the only form of corrosion due to the causticity of the EXCO solution.

Taken together with the electrochemical data, it can be concluded that the resistance to pitting corrosion, inter-granular corrosion, and exfoliation corrosion of the T76 + T6 aged 7150 Al alloy is higher than that of the 7150-T77 Al alloy.

The rationale for selecting three different solutions as electrolytes is to study various corrosion behaviors and elucidate the corrosion mechanisms. Each medium has its own specific features. As shown in Fig. 3(c), fewer potential parameters are obtained from the cyclic polarization curves of the samples in the solution of EXCO. However, the difference in the EIS of the two tempers is the most distinct in EXCO solution. Similarly, in 10 mmol/L NaCl + 0.1 mol/L Na_2SO_4, the EIS of the T76 + T6 aged 7150 Al alloy and the 7150-T77 Al alloy almost overlaps, while the difference between the pitting potentials of the two tempers is significant. The pitting potential corresponds to transient dissolution associated with the attack of the fine hardening particles and the surrounding solid solution in the thin surface layer, and to combined inter-granular and selective grain attack [27].

An φ_{ptp} was observed in 3.5% NaCl and 10 mmol/L NaCl + 0.1 mol/L Na_2SO_4 solutions. According to Refs. [9,28,29], the pit transition potential corresponds to the condition of complete repassivation for small pits, but surface repassivation for deeper pits requires further potential depression at φ_{rep}. However, this proposal was challenged by FINŠGAR and MILOŠEV [30] who believed that pitting propagation does not stop but continues at a decreasing rate until φ_{rep} is reached, therefore, making the physical meaning of φ_{ptp} be the subject of debate for years. In 1976, GALVELE [31] proposed that, at each potential, the pits in the oxide would exhibit a characteristic $x \cdot i$ value determined by the deepness of the pit and by the current density. As soon as the system reaches the minimum $x \cdot i$ value for pit growth, the pit will start to grow. According to this theory, if all smaller pits are repassivated at the φ_{ptp}, then, the deepness of these smaller pits is distributed around one certain size. Obviously, this kind of distribution cannot be true. Therefore, the φ_{ptp} does not correspond to the condition of complete repassivation of the small pits.

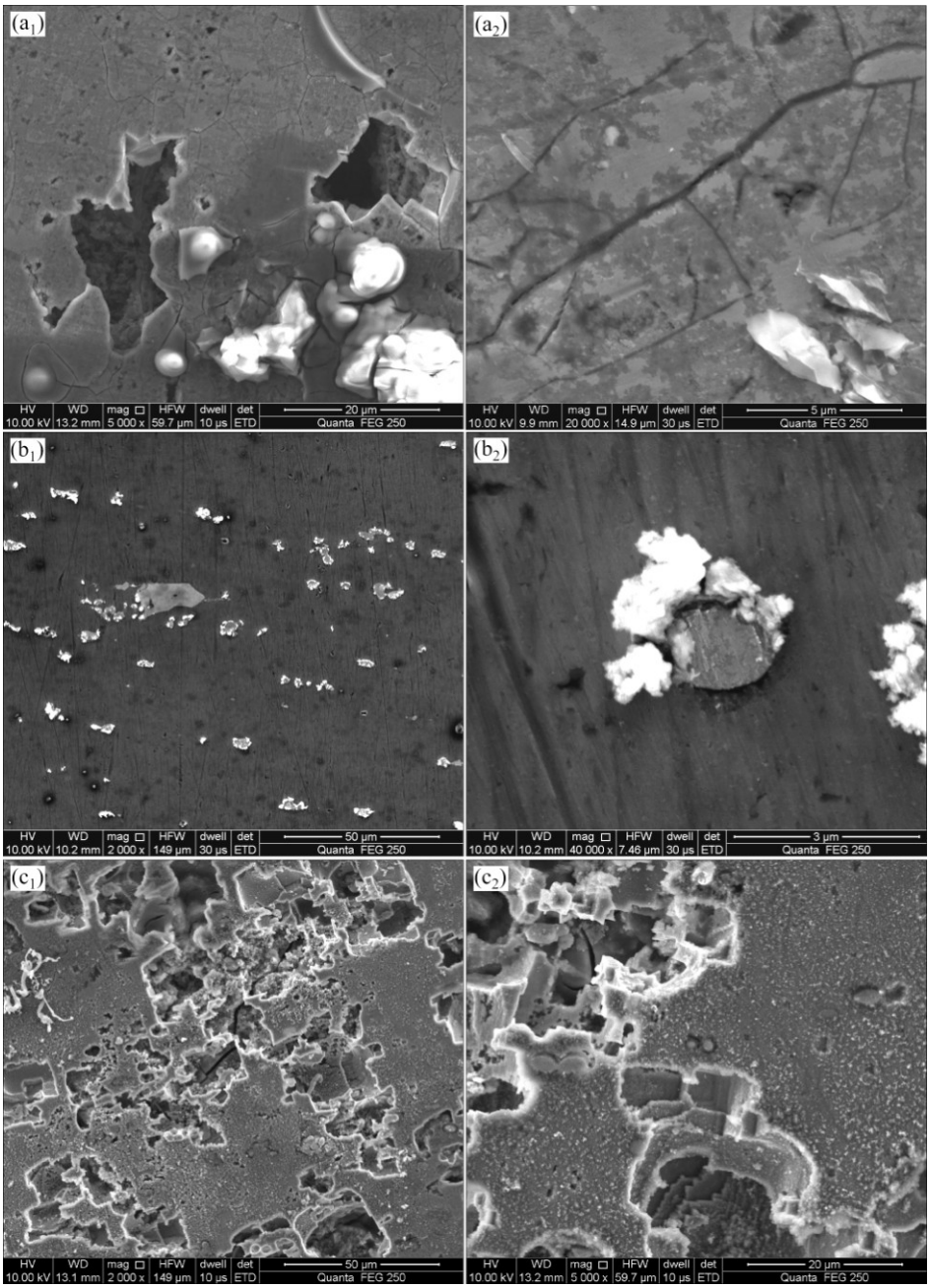

Fig. 7 SEM images of corrosion attack after OCP and cyclic polarization tests performed in 3.5% NaCl (a_1, a_2), 10 mmol/L NaCl + 0.1 mol/L Na_2SO_4 (b_1, b_2), and EXCO (c_1, c_2)

Recently, SZKLARSKA-SMIALOWSK [32] and CICOLIN et al [33] proposed that the transition onset was associated with the formation of transitory stable covalent compounds like $Al(OH)Cl_2$ and $Al(OH)_2Cl$ during repassivation which weakens the passive film and promotes further pit nucleation. The presence of φ_{ptp} in 3.5% NaCl solution suggests participation of less stable aluminium complex ions such as $AlCl^{2+}$ and $Al(OH)Cl^{+}$ in acid solution [32]. The observed increase of φ_{ptp} of the 7150-T77 Al alloy versus the T76 + T6 treated alloy suggests that the repassivation ability of the pitting pores in the alloys follows the order: T76 + T6 > T77 [28]. The steepness of the potential which decrease below φ_{ptp} can also be used to assess the severity of corrosion. For the 6082-T6 Al alloy, this parameter increases linearly with increasing the corrosion [33]. The steepness of the potential which decrease below φ_{ptp} for the T76 + T6 sample is less than that for the T77 aged sample, indicating that better corrosion resistance was achieved for the T76 + T6 aged alloy.

The mechanism of corrosion can also be roughly reflected by $\Delta\varphi$. The trend of $\Delta\varphi$ as a function of aging treatment is presented in Fig. 8. Approximate uniform corrosion (exfoliation corrosion) is observed to be the main form of corrosion in EXCO medium based on the relatively small gaps between φ_{corr} and φ_{rep}. In contrast,

localized corrosion occurs in other two solutions, as deduced from much larger $\varphi_{corr}-\varphi_{rep}$ values. Furthermore, the authors [9,28,33] previously discussed the trend of $\Delta\varphi$ as a useful method to predict the localized corrosion susceptibility of Al alloys in chloride-containing solution. From the $\Delta\varphi$ results shown in Fig. 8, we can conclude that the T76 + T6 aged 7150 Al alloy provides a larger region of passivity (larger $\varphi_{pit}-\varphi_{corr}$), with improved ability for repassivation (less $\varphi_{corr}-\varphi_{rep}$). It has also been suggested that the larger the hysteresis in the reverse scan, the more susceptible a metal is to stress cracking corrosion (SCC) [28]. The proposal is true in this case, because the T76 + T6 aged 7150 Al alloy exhibits a much higher SCC resistance than the 7150-T77 Al alloy [34].

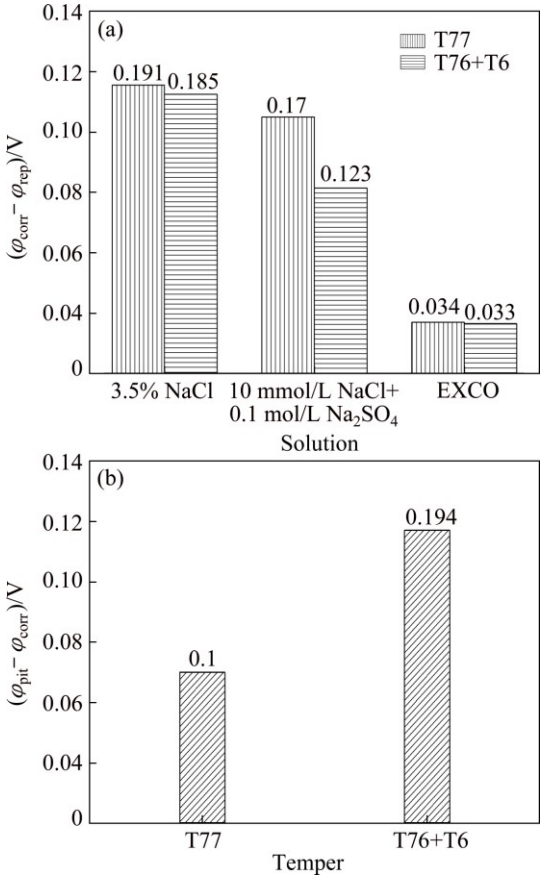

Fig. 8 $\varphi_{corr}-\varphi_{rep}$ of Al alloys in three solutions (a) and $\varphi_{pit}-\varphi_{corr}$ of Al alloys in 10 mmol/L NaCl + 0.1 mol/L Na_2SO_4 (b) as function of aging treatment

Thus far, the discussions presented above prove that the T76 + T6 aged 7150 Al alloy exhibits improved corrosion resistance compared with the alloy subjected to T77 aging treatment. However, the hardness of 7150 Al alloy should not be ignored when we investigate novel tempers. Figure 9 shows the hardness and conductivity of 7150 Al alloy as a function of the tempering process. Compared with the 7150-T77 Al alloy, surprisingly, the T76 + T6 aged 7150 Al alloy exhibits a slight increase of hardness from HV 174 to HV 176. The conductivity also increased from 29.6% IACS for T77 aged alloy to 31.5% IACS for T76 + T6 aged alloy.

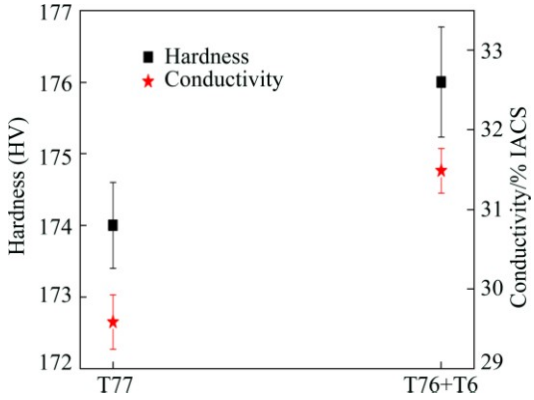

Fig. 9 Effect of tempering process on hardness and conductivity of 7150 Al alloy

The relationship between the microstructure and properties of materials is a key concern in materials science and engineering. The different microstructures revealed by TEM are shown in Fig. 10. For the RRA T77 aged alloy shown in Fig. 10(a), there is a clear discontinuous nature of η precipitates. The discontinuous distribution of the η precipitates at the grain boundary is a feature of the retrogression process [35]. The micrograph of the T76 + T6 aged 7150 alloy is similar to that of the T77 aged alloy. However, the grain boundary of the T76 + T6 aged 7150 Al alloy shown in Fig. 10(b) is characterized by the η intermetallics with a larger size and a larger interparticle spacing than that of the 7150-T77 Al alloy. This result is consistent with DONG's work on the 7055 Al alloy [36]. This is due to longer time for the over-aging process, leading to further coarsening of the $MgZn_2$ particles at the grain boundary.

The usual precipitation sequence of Al–Zn–Mg–(Cu) alloys can be summarized as follows [7,37]: solid solution → GP zones → metastable η' precipitates → stable η ($MgZn_2$) precipitates, where the GP zones (coherent with matrix) and η' precipitates (semi-coherent with matrix) have an important impact on the strength, while η precipitates (incoherent) has little effect on the strength. LI et al [35] found that the 7150 Al alloy possesses a strength as high as that of the conventional 7150-T6 alloy prepared by retrogressing at 175 °C with the retrogression time extending to 3 h. They proposed that the 7150-T6 alloy is mainly strengthened by fine GP zones with high density, while the intra-grain microstructure of 7150-RRA retrogressed at 175 °C for 3 h or 195 °C for 1 h is characterized by relatively coarseη' precipitates. As shown in Fig. 10(b), there are no coarse η precipitates in the intra-grain. Thus, it can be concluded that the sample subjected to T76 + T6 aging

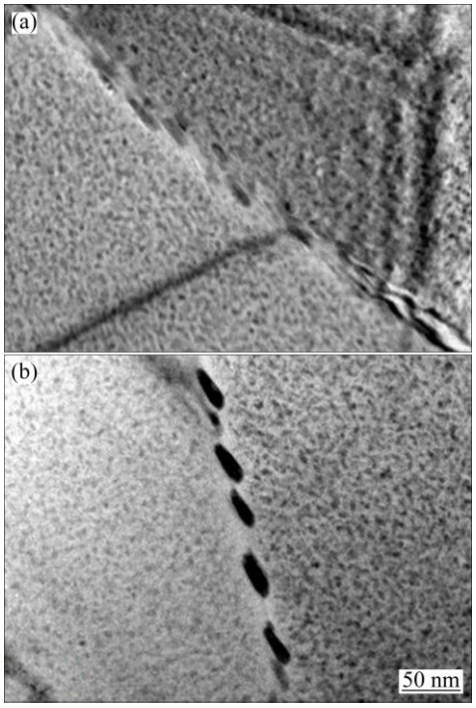

Fig. 10 TEM images of 7150 Al alloy subjected to T77 (a) and T76 + T6 (b) aging processes

process at a lower retrogression temperature over a longer retrogression time is also mainly strengthened by η' precipitates. The slight increase of strength for the T76 + T6 aged sample is attributed to more η' precipitates, leading to a decline of the Zn and Mg contents of the matrix. Furthermore, the increase of the electrical conductivity is caused by the decline of the Zn and Mg contents of the matrix and further coarsening of the grain boundary particles (GBPs) [7,36,38].

In ultra-high strength Al−Zn−Mg−Cu alloys, the strength is determined by intra-granular precipitations and the corrosion behavior is associated with GBPs. Pitting corrosion, inter-granular corrosion (IGC) and SCC are directly related to the morphology and distribution of the GBPs. The GBPs of the Al−Zn−Mg−Cu alloys are η phases, which are anodic to the Al matrix and dissolve preferentially. For the T6 aged Al−Zn−Mg−Cu alloys, the η phases are continuously distributed along the high angle recrystallized grain boundaries and become the channel for SCC and IGC. Compared with peak aging T6, T77 increases the corrosion resistance of the 7150 Al alloy due to coarsening and spacing of the GBPs [4,5,35]. When the retrogression temperature is lower than the solution temperature of the η precipitates, but higher than the re-aging temperature, the η precipitates congregate and coarsen. The grain boundary η precipitates are coarser than those in the 7150-T6 Al alloy, resulting in the inhibition of further development of the ICG and SCC. Further coarsening of the GBPs often means better corrosion resistance [5,14]. By lowering the retrogression temperature to 160 °C and extending the retrogression time to 8 h, further coarsening of the η precipitates in the grain boundaries was obtained, leading to improved corrosion resistance.

5 Conclusions

1) The electrochemical parameters deduced from cyclic polarization curves (J_{corr}, J_{rep}, R_{corr} and R_{rep}) and EIS (R_p or R_{ct}) indicate that the corrosion rate of 7150-T77 Al alloy is higher than that of T76 + T6 aged 7150 alloy.

2) Together with the hardness and corrosion morphology results, it can be concluded that, compared with the conventional T77 treatment, the novel T76 + T6 aging process not only maintains the high strength of the 7150 extruded Al alloy, but also increases its resistance to pitting corrosion, inter-granular corrosion and exfoliation corrosion.

3) The improved corrosion resistance is associated with further coarsening and interspacing of the grain boundary particles.

References

[1] DURSUN T, SOUTIS C. Recent developments in advanced aircraft aluminium alloys [J]. Materials and Design, 2014, 56: 862−871.

[2] SUN Qing-qing, CHEN Kang-hua, CHEN Qi-yuan. Influence of heat treatments on electrochemical corrosion behaviours of aircraft Al alloy with Yb micro-alloy [J]. The Chinese Journal of Nonferrous Metals, 2016, 26(3): 479−485. (in Chinese)

[3] CINA B. Reducing the susceptibility of alloys, particularly aluminium alloys, to stress corrosion cracking. US: 3856584 [P]. 1974.

[4] PENG G, CHEN K, CHEN S, FANG H. Influence of repetitious-RRA treatment on the strength and SCC resistance of Al−Zn−Mg−Cu alloy [J]. Materials Science and Engineering A, 2011, 528(12): 4014−4018.

[5] PENG G S, CHEN K H, CHEN S Y, FANG H C. Influence of dual-RRA temper on the exfoliation corrosion and electrochemical behavior of Al−Zn−Mg−Cu alloy [J]. Materials and Corrosion, 2013, 64(4): 284−289.

[6] VIANA F, PINTO A, SANTOS H, LOPES A. Retrogression and re-ageing of 7075 aluminium alloy: Microstructural characterization [J]. Journal of Materials Processing Technology, 1999, 92: 54−59.

[7] MARLAUD T, DESCHAMPS A, BLEY F, LEFEBVRE W, BAROUX B. Evolution of precipitate microstructures during the retrogression and re-ageing heat treatment of an Al−Zn−Mg−Cu alloy [J]. Acta Materialia, 2010, 58(14): 4814−4826.

[8] CHAKRABARTI D J, GOODMAN J H, KRIST C M, LIU J, SAWTELL R R, VENEMA G B, WESTERLUND R W. Aluminum alloy products having improved property combinations and method for artificially aging same. US: 8840737 [P]. 2005.

[9] TRUEBA M, TRASATTI S P. Study of Al alloy corrosion in neutral NaCl by the pitting scan technique [J]. Materials Chemistry and Physics, 2010, 121(3): 523−533.

[10] MARLAUD T, MALKI B, DESCHAMPS A, BAROUX B. Electrochemical aspects of exfoliation corrosion of aluminium alloys: The effects of heat treatment [J]. Corrosion Science, 2011, 53(4): 1394−1400.

[11] TRDAN U, GRUM J. Evaluation of corrosion resistance of AA6082-T651 aluminium alloy after laser shock peening by means

of cyclic polarisation and EIS methods [J]. Corrosion Science, 2012, 59: 324−333.
[12] ARRABAL R, MINGO B, PARDO A, MOHEDANO M, MATYKINA E, RODR GUEZ I. Pitting corrosion of rheocast A356 aluminium alloy in 3.5 wt.% NaCl solution [J]. Corrosion Science, 2013, 73: 342−355.
[13] DAV B, de DAMBORENEA J. Use of rare earth salts as electrochemical corrosion inhibitors for an Al−Li−Cu (8090) alloy in 3.56% NaCl [J]. Electrochimica Acta, 2004, 49(27): 4957−4965.
[14] FANG H, CHEN K, CHEN X, CHAO H, PENG G. Effect of Cr, Yb and Zr additions on localized corrosion of Al−Zn−Mg−Cu alloy [J]. Corrosion Science, 2009, 51(12): 2872−2877.
[15] WLOKA J, VIRTANEN S. Influence of scandium on the pitting behavior of Al−Zn−Mg−Cu alloys [J]. Acta Materialia, 2007, 55(19): 6666−6672.
[16] ASHASSI-SORKHABI H, GHASEMI Z, SEIFZADEH D. The inhibition effect of some amino acids towards the corrosion of aluminum in 1M HCl+1M H_2SO_4 solution [J]. Applied Surface Science, 2005, 249(1): 408−418.
[17] UMOREN S, OBOT I, EBENSO E, OBI-EGBEDI N. The Inhibition of aluminium corrosion in hydrochloric acid solution by exudate gum from “Raphia hookeri” [J]. Desalination, 2009, 247(1): 561−572.
[18] KEDDAM M, KUNTZ C, TAKENOUTI H, SCHUSTERT D, ZUILI D. Exfoliation corrosion of aluminium alloys examined by electrode impedance [J]. Electrochimica acta, 1997, 42(1): 87−97.
[19] HUANG L, CHEN K, LI S, SONG M. Influence of high-temperature pre-precipitation on local corrosion behaviors of Al−Zn−Mg alloy [J]. Scripta Materialia, 2007, 56(4): 305−308.
[20] SUN Qing-qing, DONG Peng-xuan, SUN Rui-ji, CHEN Qi-yuan, CHEN Kang-hua. The effect of ageing processes on electrochemical corrosion of Al−6.2Zn−2.3Mg−2.3Cu extruded aluminium alloy [J]. The Chinese Journal of Nonferrous Metals, 2015, 25(4): 866−874. (in Chinese)
[21] MACDONALD D, SONG H, MAKELA K, YOSHIDA K. Corrosion potential measurements on type 304 SS and alloy 182 in simulated BWR environments [J]. Corrosion, 1993, 49(1): 8−16.
[22] SEKINE I, KAWASE T, KOBAYASHI M, YUASA M. The effects of chromium and molybdenum on the corrosion behavior of ferritic stainless steels in boiling acetic acid solutions [J]. Corrosion Science, 1991, 32(8): 815−825.
[23] JANIK-CZACHOR M. Stability of the passive state of Ni−Zr glassy alloys [J]. Corrosion, 1993, 49(9): 763−768.
[24] SUN Qing-qing, CHEN Qi-yuan, CHEN Kang-hua. The effect of concentration of chloride ion, temperature and applied stress on the electrochemical corrosion behavior of 7B50 Al alloy [C]//Conference of Marine Materials Corrosion and Protection. Beijing: Chinese Society of Corrosion and Protection, 2014: 331−336. (in Chinese)
[25] SUN Qing-qing, SUN Rui-ji, CHEN Song-yi, CHEN Qi-yuan, CHEN Kang-hua. Effect of atmospheric pollutants on electrochemical corrosion behavior of 7B50 aluminium alloy [J]. The Chinese Journal of Nonferrous Metals, 2015, 25(3): 575−581. (in Chinese)
[26] KOCIJAN A, MERL D K, JENKO M. The corrosion behavior of austenitic and duplex stainless steels in artificial saliva with the addition of fluoride [J]. Corrosion Science, 2011, 53(2): 776−783.
[27] MENG Q, FRANKEL G. Effect of Cu content on corrosion behavior of 7xxx series aluminum alloys [J]. Journal of the Electrochemical Society, 2004, 151(5): B271−B283.
[28] YASUDA M, WEINBERG F, TROMANS D. Pitting corrosion of Al and Al−Cu single crystals [J]. Journal of the Electrochemical Society, 1990, 137(12): 3708−3715.
[29] PICKERING H W. Whitney award lecture−1985: On the roles of corrosion products in local cell processes [J]. Corrosion, 1986, 42(3): 125−140.
[30] FINŠGAR M, MILOŠEV I. Corrosion behavior of stainless steels in aqueous solutions of methanesulfonic acid [J]. Corrosion Science, 2010, 52(7): 2430−2438.
[31] GALVELE J R. Transport processes and the mechanism of pitting of metals [J]. Journal of the Electrochemical Society, 1976, 123(4): 464−474.
[32] SZKLARSKA-SMIALOWSKA Z. Pitting corrosion of aluminum [J]. Corrosion Science, 1999, 41(9): 1743−1767.
[33] CICOLIN D, TRUEBA M, TRASATTI S. Effect of chloride concentration, pH and dissolved oxygen, on the repassivation of 6082-T6 Al alloy [J]. Electrochimica Acta, 2014, 124: 27−35.
[34] LIU Wei. Effect of aging treatment on microstructure and properties of 7150 aluminium alloy plates [D]. Changsha: Central South University, 2015. (in Chinese)
[35] LI J F, BIRBILIS N, LI C X, JIA Z Q, CAI B, ZHENG Z Q. Influence of retrogression temperature and time on the mechanical properties and exfoliation corrosion behavior of aluminium alloy AA7150 [J]. Materials Characterization, 2009, 60(11): 1334−1341.
[36] DONG Peng-Xuan. Research on multiphase microstructure modulation and properties of Al−8.54Zn−2.41Mg−*x*Cu aluminium alloy [D]. Changsha: Central South University, 2013. (in Chinese)
[37] STILLER K, WARREN P, HANSEN V, ANGENETE J, GJϕNNES J. Investigation of precipitation in an Al−Zn−Mg alloy after two-step ageing treatment at 100 °C and 150 °C [J]. Materials Science and Engineering A, 1999, 270(1): 55−63.
[38] ANDREATTA F, TERRYN H, de WIT J H W. Corrosion behavior of different tempers of AA7075 aluminium alloy [J]. Electrochimica acta, 2004, 49(17): 2851−2862.

使用新型三级时效制度改善 7150 铝合金耐腐蚀性能

孙睿吉[1]，孙擎擎[1,2,3]，谢跃煌[1]，董朋轩[1]，陈启元[2]，陈康华[1]

1. 中南大学 粉末冶金国家重点实验室，长沙 410083；2. 中南大学 化学化工学院，长沙 410083；
3. School of Chemical Engineering, Purdue University, West Lafayette 47907, IN, USA

摘　要：对比研究一种新型三级时效制度(T76+T6)和常规回归再时效制度(RRA T77)对 7150 铝合金型材耐腐蚀性能的影响。选取三种腐蚀溶液(3.5% NaCl; 10 mmol/LNaCl+0.1 mol/L Na_2SO_4; 4 mol/LNaCl + 0.5 mol/L KNO_3 + 0.1 mol/L HNO_3)，分别对 7150 铝合金型材进行开路电位、循环极化曲线以及电化学阻抗谱的表征。讨论自腐蚀电位、点蚀电位、点蚀转换电位以及电位差值等参数对铝合金腐蚀表征的适用性与局限性。电化学与扫描电镜(SEM)结果表明，相比于传统 RRA T77 制度，T76 + T6 时效制度处理的铝合金在没有强度损失的前提下，具备更好的耐点蚀、耐晶间腐蚀以及耐剥落腐蚀的能力。这是由于该新型三级时效制度处理的铝合金的晶界析出相进一步粗化和断续分布所致。

关键词：7150 铝合金；新型三级时效；循环极化曲线；电化学阻抗谱

(Edited by Mu-lan QIN)